Since January 2020 Elsevier has created a COVID-19 resource centre with free information in English and Mandarin on the novel coronavirus COVID-19. The COVID-19 resource centre is hosted on Elsevier Connect, the company's public news and information website.

Journal of Photochemistry and Photobiology 10 (2022) 100120

Contents lists available at ScienceDirect

Journal of Photochemistry and Photobiology

journal homepage: www.sciencedirect.com/journal/journal-of-photochemistry-and-photobiology

UV inactivation of Semliki Forest virus and *E. coli* bacteria by alternative light sources

Atis Skudra [a], Gita Revalde [a,d,*], Anna Zajakina [b], Linda Mezule [c], Karina Spunde [b], Talis Juhna [c], Kristiana Rancane [a]

[a] Institute of Atomic Physics and Spectroscopy, University of Latvia, Riga, Jelgavas str.3, LV-1004, Latvia
[b] Latvian Biomedical Research and Study Centre, Ratsupites iela 1, Riga, LV-1067, Latvia
[c] Water Research and Environmental Biotechnology Laboratory, Riga Technical University, Kalku str 1, Riga, LV-1658, Latvia
[d] Institute of Technical Physics, Riga Technical University, Kalku str 1, Riga, LV-1658, Latvia

ARTICLE INFO

Keywords:
UV disinfection
Inactivation
Virus restriction
Reduction
UV light sources
Electrodeless lamps
Escherichia coli
Semliki forest virus
UV-C
Pandemic

ABSTRACT

The quick spreading of the SARS-CoV-2 virus, initiating the global pandemic with a significant impact on economics and health, highlighted an urgent need for effective and sustainable restriction mechanisms of pathogenic microorganisms. UV-C radiation, causing inactivation of many viruses and bacteria, is one of the tools for disinfection of different surfaces, liquids, and air; however, mainly mercury 254 nm line is commonly used for it. In this paper, we report our results of the experiments with newly elaborated special type polychromatic non-mercury UV light sources, having spectral lines in the spectral region from 190 nm to 280 nm. Inactivation tests were performed with both *Escherichia coli* (*E.coli*) bacteria and Semliki Forest virus (SFV) as a representative of human enveloped RNA viruses. In addition, the effect of prepared lamps on virus samples in liquid and dry form (dried virus-containing solution) was tested. Reduction of 4 log10 of *E.coli* was obtained after 10 min of irradiation with both thallium-antimony and arsenic high-frequency electrodeless lamps. High reduction results for the arsenic light source demonstrated sensitivity of *E. coli* to wavelengths below 230 nm, including spectral lines around 200 nm. For the Semliki Forest virus, the thallium-antimony light source showed virus inactivation efficiency with a high virus reduction rate in the range of 3.10 to $>$ 4.99 log10 within 5 min of exposure. Thus, the new thallium-antimony light source showed the most promising disinfection effect in bacteria and viruses, and arsenic light sources for bacteria inactivation, opening doors for many applications in disinfection systems, including for pathogenic human RNA viruses.

1. Introduction

The COVID-19 pandemic has had a significant influence on economics, health, and also technologies. The rapid spreading of the illness activated all kinds of research for appropriate disinfection tools for air and surfaces [1,2]. Electromagnetic radiation with wavelengths from 200 nm to 280 nm (UV-C radiation) is one of the well-known tools for disinfection of different surfaces, liquids, and air. It is known to be also very energy-efficient [3]. When used for disinfection, this radiation has various advantages over liquid disinfectants and heat sterilization. In addition, UV- C light sources are recognised as promising tools for respiratory disinfection [4]. These aspects play an important role both in everyday disinfection procedures and in the fight against global pandemics.

The exact mechanism by which UV-C radiation causes inactivation of viruses and bacteria is still being discussed and studied, but UV-C is known to damage cell material (including DNA/RNA) [5]. Damage mechanisms of nucleic acids are discussed, for example, in [6,7], damage of proteins in [8], as well as internal production of oxygen radicals in [9]. One of the mechanisms causing the inactivation of pathogens is diminishing their replication by forming pyrimidine dimers when absorbing UV-C light [10]. It has been shown that the effect of ultraviolet radiation strongly depends on the spectral structure of the light or radiation frequency. The radiation within the ultraviolet region from 240 nm to 280 nm (more precisely, the absorption peak near 260 nm that overlaps with the absorption peak of genetic material) inactivates microorganisms, harming their genetic material [11,12]; higher frequencies (lower wavelengths) affect also proteins [7].

However, the potential of UV disinfection is not fully exploited. Mainly low-pressure mercury lamps have been used in most disinfection experiments as UV-C light sources. The "working" spectral line in such lamps is the mercury resonance line of 253.7 nm wavelength, located

* Correspondence author.
E-mail address: gitar@latnet.lv (G. Revalde).

https://doi.org/10.1016/j.jpap.2022.100120

Available online 10 April 2022

near the maximum of the DNA absorption band [3,13]. UV-C 253.7 nm light is absorbed by RNA/DNA, which advances the formation of pyrimidine dimers, e.g., uracil dimers [3]. There are not so many experiments applying other wavelengths. Experiments with maximums at 222 nm [14,15], 365 nm, 207 nm, as well as ultraviolet light-emitting diodes, with wavelengths, for example, 265, 280, 300 nm [9,16] have been reported. However, despite laboratory scale demonstrations, critical drawbacks of the sources e.g. limited LED output power [1], impeded their widespread use in real conditions [17].

The dominant application of mercury 253.7 nm wavelength in disinfection is caused by the broad availability of mercury light sources. They are relatively inexpensive, and their production is widely developed. The lack of other appropriate ultraviolet radiation sources is the main restricting factor for using other UV spectral lines [18].

In addition, the light of mercury lamps has been reported as carcinogenic and catarctogenic [19]. By contrast, far UV-C radiation in the range from 205 to 222 nm effectively inactivates bacteria without damaging uncovered skin [15]. The problem of mercury reduction is well known in the light source industry [20,21]. Serious commitments have been made to eliminate toxic lighting through the Minamata Convention on Mercury, which is ratified by 50 countries [22]. To reduce the use of toxic mercury, the possibility to replace Hg vapor lamps by 222 nm excimer lamps or 270 nm LEDs has been proposed; however, this should be investigated in more detail in the future. In addition, short-wavelength UV-LEDs are costly and have low intensity [16].

It should be also mentioned that shorter UV wavelengths exhibit greater photon energy. Researchers [5] emphasised the need for further research to develop appropriate light sources for the inactivation of human pathogenic viruses, including SARS-CoV-2. Questions to clarify are connected with all aspects, including efficacy, environment, lifetime, costs, safety, etc.

Polychromatic lamps, compared to monochromatic lamps, may possess greater efficiency by activating several damaging mechanisms [8,23,24]. It is presumed that the differences in the inactivation indicate that monochromatic mercury UV-C lamps only activate genetic damage, whereas polychromatic light sources also affect proteins [24].

In this paper, we present new, special polychromatic UV light sources and the results of the inactivation tests with selected bacteria and viruses. High-frequency electrodeless light sources (HFELs) are bright radiators of intense UV spectral lines [25,26]. HFELs must be optimised and tested for each special application. Up to now, HFELs have been optimised for usage, for example, in atomic absorption spectrometers [27]. HFELs can be filled with different elements such as lead, phosphor, selenium, arsenic, thallium, antimony, mercury, and others, easily changing the spectral composition of radiation. An inductively coupled HF discharge is initiated using outside electrodes. The proposed HFELs have significant advantages in comparison with other UV-C light sources (Tables 1, ST1). These HFELs emit spectral lines also hitting the RNA/DNA absorption band below 220 nm (there are very few light sources offered that cover this spectral region) [17, Fig, 1a]. In addition, the geometry of lamps is flexible, and they can be manufactured in different forms.

In this paper, results of inactivation experiments of *E. coli* bacterium and Semliki Forest virus, a representative of human enveloped RNA viruses, with arsenic, lead, selenium, thallium-antimony, and mercury HFELs are reported. The effect of the prepared lamps on virus samples in liquid and dry form (dried virus-containing solution) was tested.

2. Materials and methods

2.1. UV light sources

For this work, arsenic, selenium, lead, thallium-antimony HFELs were manufactured in our laboratory, using previously elaborated technology [28–30]. The HFELs were made of fused silica and filled with a working element (selected metal vapor), and some rare gas, typically - argon at 400 Pa (3 Torr) pressure (Fig. 1).

An outer electromagnetic field of about 100 MHz frequency is applied to initiate a discharge inside the lamp. Table 1 illustrates the main features of the HFELs.

In this experiment, we used spherical lamp bulbs of 1 cm diameter. In general, lamps can be made in different forms and sizes, taking into account the requirements of the system.

Spectra of the manufactured HFELs were recorded and monitored using a high-resolution spectrometer (Jobin Yvon 1000 M; holographic grating 1800 gr/mm) with Synapse Plus CCD head (with 2048 × 512-pixel front-illuminated CCD UV/Visible chip), thermoelectrically cooled to −75 °C.

The spectra of the ultraviolet region of thallium-antimony, arsenic, lead, selenium, and mercury HFELs are illustrated in Figs. 2-6. In Fig. 6, a typical mercury monochromatic spectrum can be seen with one strong 253.7 nm spectral line, located at the side of the absorbance curve of DNA at 260 nm (DNA and RNA have similar absorbance curves) [13].

Thallium-antimony, arsenic, lead, and selenium spectra (Figs. 2–5) consist of many emission lines, permitting wider interaction with the RNA/DNA absorption band around 260 nm, hitting the higher absorption peak around 200 nm, as well as activating other damaging mechanisms with the light below 220 nm.

HFEL with Tl-Sb (Fig. 2) emits many lines in the region 250 nm - 280 nm and some below 230 nm. The most intensive line is at 277 nm. The emission spectrum of the arsenic light source (Fig. 3) contains intense spectral lines in the region 230 nm - 286 nm and in the far UV-C region and beyond it at 194 nm, 197 nm, 200 nm wavelength (Supplementary material, Fig. S1).

The lead HFEL (Fig. 4) emits many spectral lines in the region from 240 nm to 280 nm and several strong lines below 230 nm.

The most intense selenium lines are located in the region 196 nm - 216 nm, and only two weaker 241 nm and 254 nm lines around RNA/DNA absorption band at 260 nm.

2.2. Irradiation

Irradiation measurements were performed using calibrated Ocean Optics high-resolution spectrometer HR4000+ (spectral range 200 - 1100 nm, spectral resolution 0.47 nm) in the same set-up as used for inactivation (Fig. 7, 1), after completion of inactivation measurements.

The HFELs were mounted in a holder, and a lens was used for obtaining a parallel beam of light, thus ensuring that the perpendicular planar plane was uniformly irradiated. The lens was placed at a distance of 6 cm from the irradiation surface (Fig. 7,1). The illuminated area was a circle of 3 cm in diameter. The lamp operation conditions were kept constant throughout the experiments. The stability of the HFELs can be characterised by the ratio $\frac{\Delta I}{I} = 5 \times 10^{-5}$ per hour for measurement time 5000 h, where ΔI - a shift of intensity and I is intensity [31]. Also, our previous measurements confirm the high stability of the lamps [32].

Calibration of the spectrometer was performed with a NIST-traceable calibrated reference lamp for the UV region (Ocean Optics, deuterium-halogen light source DH-2000 Cal, 200 - 400 nm). A high-sensitivity CCD was used as a detector (2048-elements).

The light was received by the cosine corrector (CC-3-UV-S, Ocean Optics) that was attached to the end of the solarisation-resistant optical fiber of 200 μm diameter (OP200–2-SR-BX) and transmitted to the calibrated spectrometer. As a result, spectra in absolute units, μW/cm^2/nm, were registered. To obtain the irradiance in units of μW/cm^2, integration was performed over the respective spectral lines in the UV-C region from 200 - 280 nm. The uniformity of the illumination was ensured by measuring the irradiation in 5 points across the illuminated area (Fig. 7, 2). The intensity varied for different lamps about 8 - 10%. Standard deviations were calculated (see Results and discussion).

Viruses and bacteria exposed to UV irradiation are subject to an

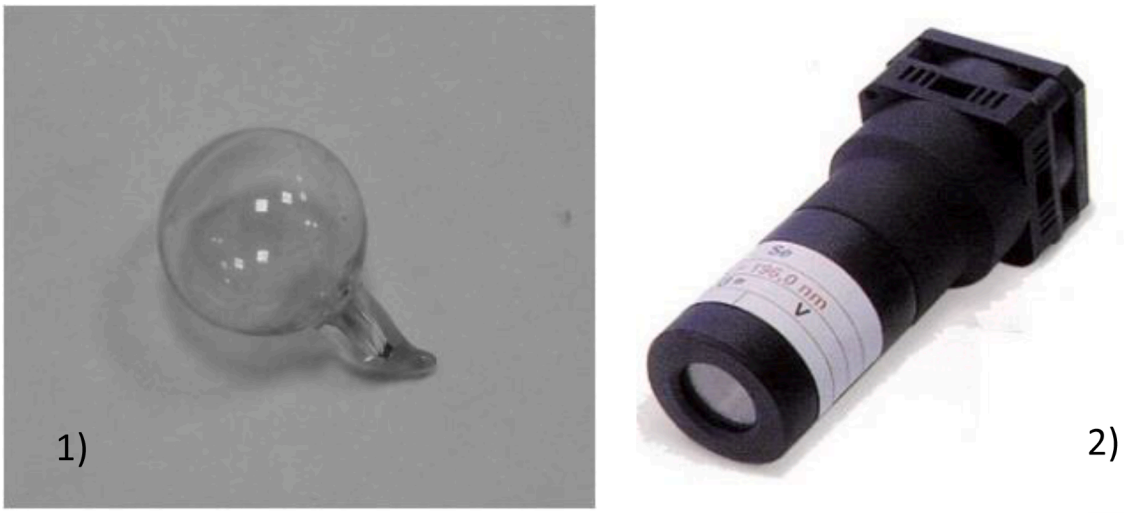

Fig. 1. 1) Typical design of a light source bulb, 2) Design of an HFEL together with generator.

Table 1
Main features of the HFELs.

High-frequency electrodeless lamps	Operation parameters
Spectral properties	Polychromatic with many spectral lines in the region 190 - 280 nm (including lines below 220 nm)
Filling	Different filling possibilities
Filling option	Mercury-free
Geometry	Flexible geometry at different scales
Power supply	Low power supply (<30 V, 1A)
Warm-up time	Short warm-up time <5 min
Working time	Long working life due to outer electrodes (40,000 −60,000 h) [31]

exposure dose (fluence) D that is a function of the irradiance I_R multiplied by the exposure time t, as follows [12]:

$$D = t \times I_R \tag{1}$$

where D - UV exposure dose (fluence), mJ/cm^2; t -exposure time, s; I_R-irradiance, mW/cm^2 (the radiative flux through a flat surface).

UV rate constant k can be estimated from the first order decay equation [12].

$$N(t) = N(0)e^{-kD}, \tag{2}$$

where $N(t)$ is the total virus titre at time t *(s),* $N(0)$ is the initial total titre at time $t = 0$, D is the dose (mWsec/cm^2 or mJ/cm^2) or it is equal to radiant flux (mW/cm^2) multiplied by t in seconds, k is the rate constant

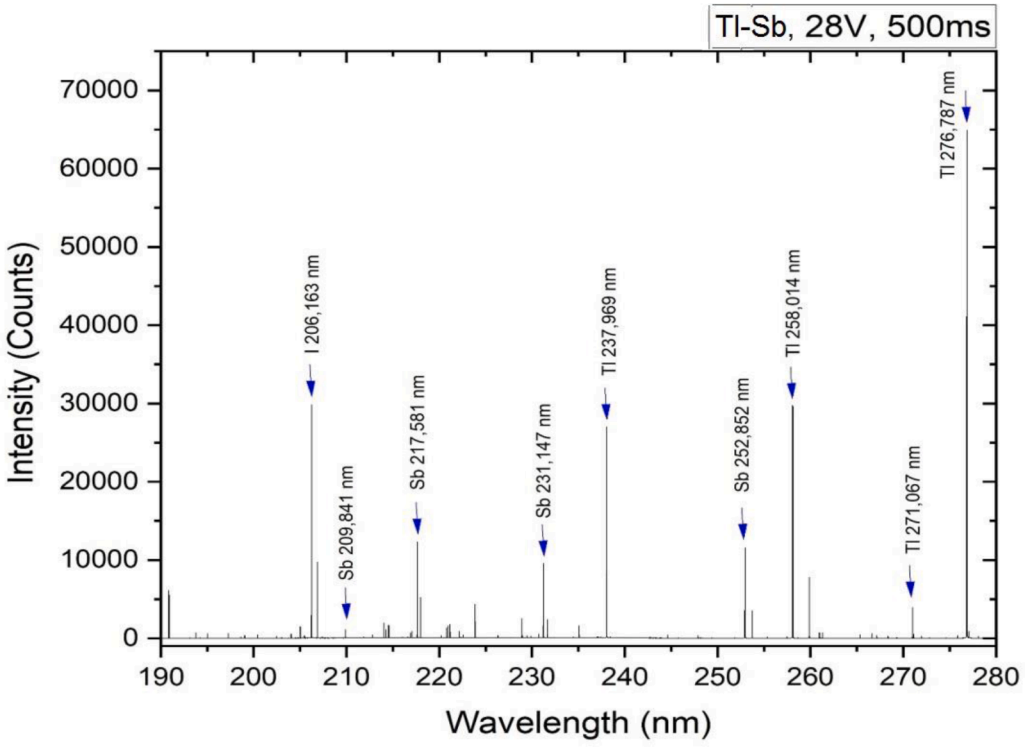

Fig. 2. The spectrum of a Tl-Sb HFEL from 190 - 280 nm.

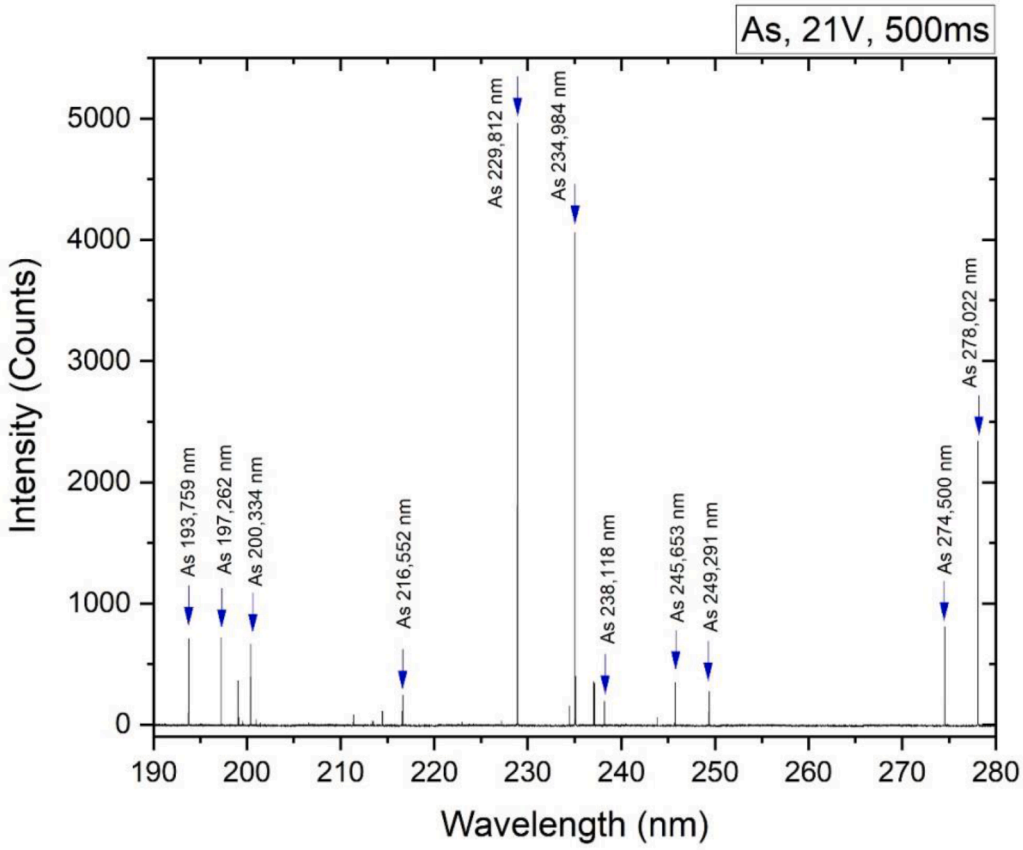

Fig. 3. The spectrum of an arsenic HFEL from 190 −280 nm.

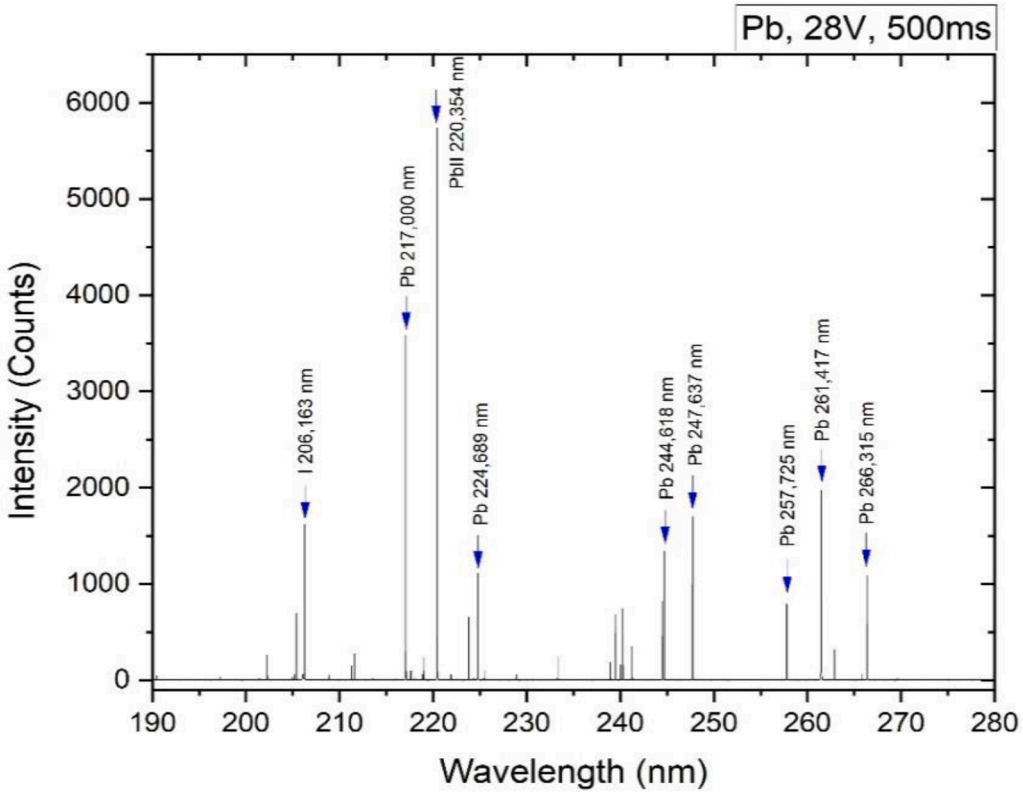

Fig. 4. The spectrum of a lead HFEL from 190 - 280 nm (Pb II - Pb ionic line).

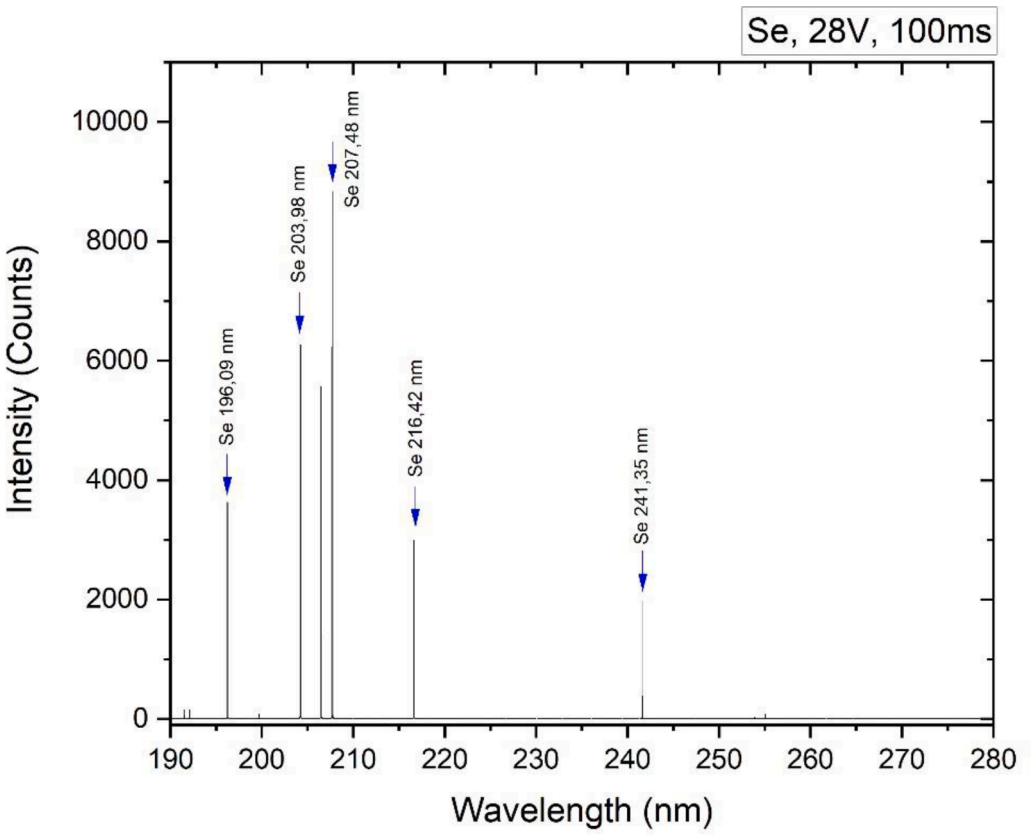

Fig. 5. The spectrum of a selenium HFEL from 190 −280 nm.

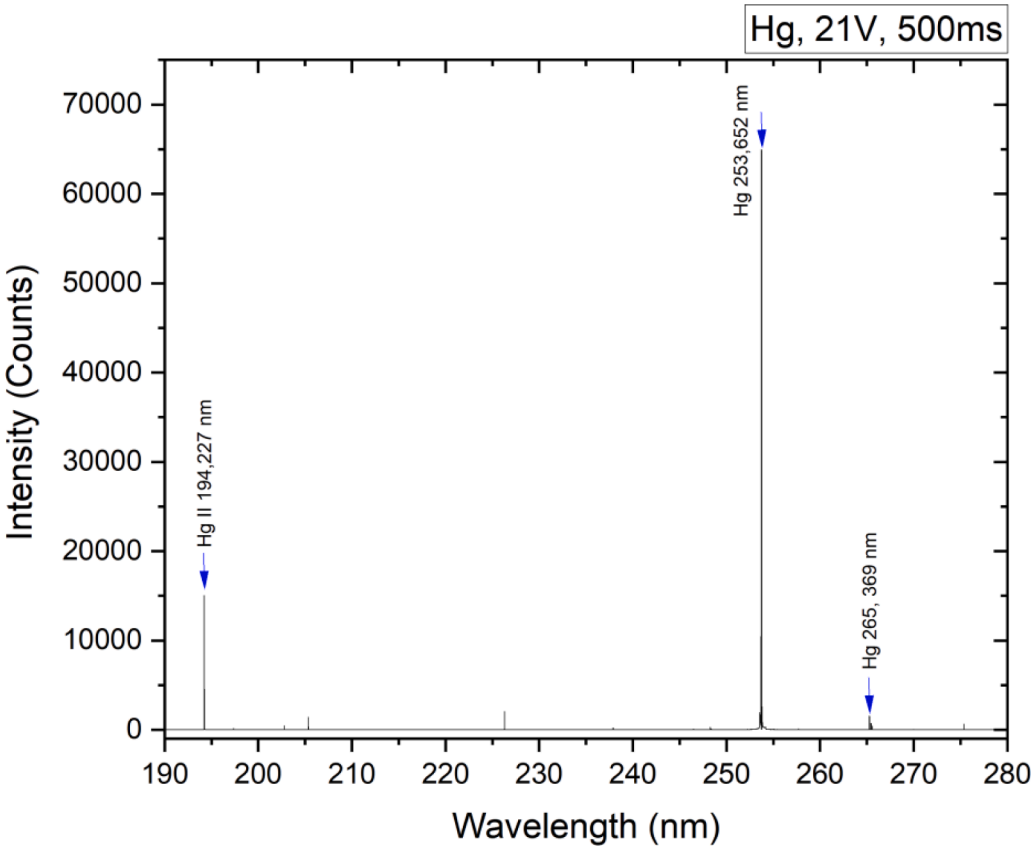

Fig. 6. The spectrum of a mercury HFEL from 190 - 280 nm (Hg II denotes an ionic spectral line).

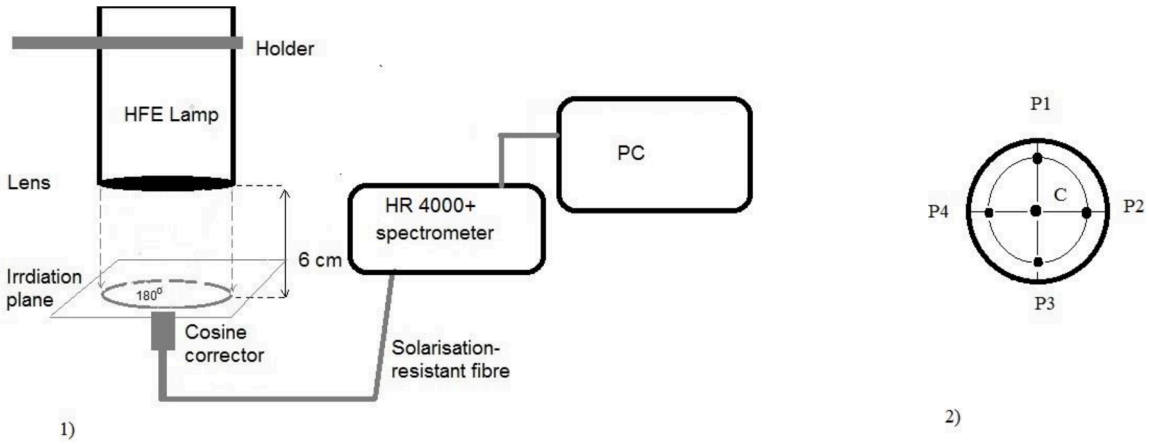

Fig. 7. 1) The set-up for the irradiation measurements, 2) HFEL intensity measurement geometry in 5 positions across the illuminated area.

for disinfection of dispersed virus particles (cm^2/mW/s).

Rate constant k can be obtained from (2):

$$k = -\frac{1}{D} ln\left(\frac{N(t)}{N(0)}\right) \; or \; k = -\frac{1}{D}\ln(S), \tag{3}$$

where S is the survival fraction.

Since the relationship between UV dose D and the natural logarithm of the survival fraction S is linear in the majority of cases, the effect of UV irradiation on any given virus can be described by the value of k. The survival fraction relationship to log reduction is given by the following equation:

$$S = \frac{1}{10^A}, \tag{4}$$

where A is log10 reduction in a number of virus titre.

2.3. Virus preparation and disinfection settings

The recombinant Semliki Forest virus (SFV) pSFVenh/Luc, encoding the firefly luciferase gene, was formed as reported previously [33,34]. Briefly, for the synthesis of infectious replication-deficient vector particles, the BHK-21 cells (Baby hamster kidney cells) were electroporated with both the recombinant viral RNA (pSFVenh/Luc) and the SFV helper RNA, providing a synthesis of SFV structural proteins. After 48 h incubation, the virus-containing medium was harvested, rapidly frozen, and subsequently used as a virus stock. The virus stock did not contain the replication-competent wild-type virus as confirmed by cell reinfection. The pSFVenh/Luc viral particles were additionally purified and concentrated by ultracentrifugation through two sucrose cushions.

The virus titre expressed in infectious units (i.u.) was quantified by infecting BHK-21 cells with serial dilutions of the virus followed by immunostaining with rabbit polyclonal antibodies specific to the nsp1 subunit of SFV replicase, as earlier reported [35].

Fig. 8 demonstrates a schematic illustration of the virus illumination test. One day before the illumination test, the BHK-21 cells were seeded into 24-well plate 4×10^4 cells per well for the SFV infection experiment, to achieve the 70% cell monolayer confluency. The next day 200 µl of virus sample in PBS buffer at 1×10^7 i.u./ml was poured into 1 well of an empty sterile 24-well plate (surface area 1.9 cm^2). Alternatively, 10 µl of virus solution in PBS at a concentration of 2×10^7 i.u./ ml was poured into the well of an empty sterile 96-well plate (surface area 0.32 cm^2). The dry virus sample was prepared in a 24-well plate by drying 20 µl of virus solution in a DMEM at a concentration of 1×10^8 i.u./ml for one hour at room temperature.

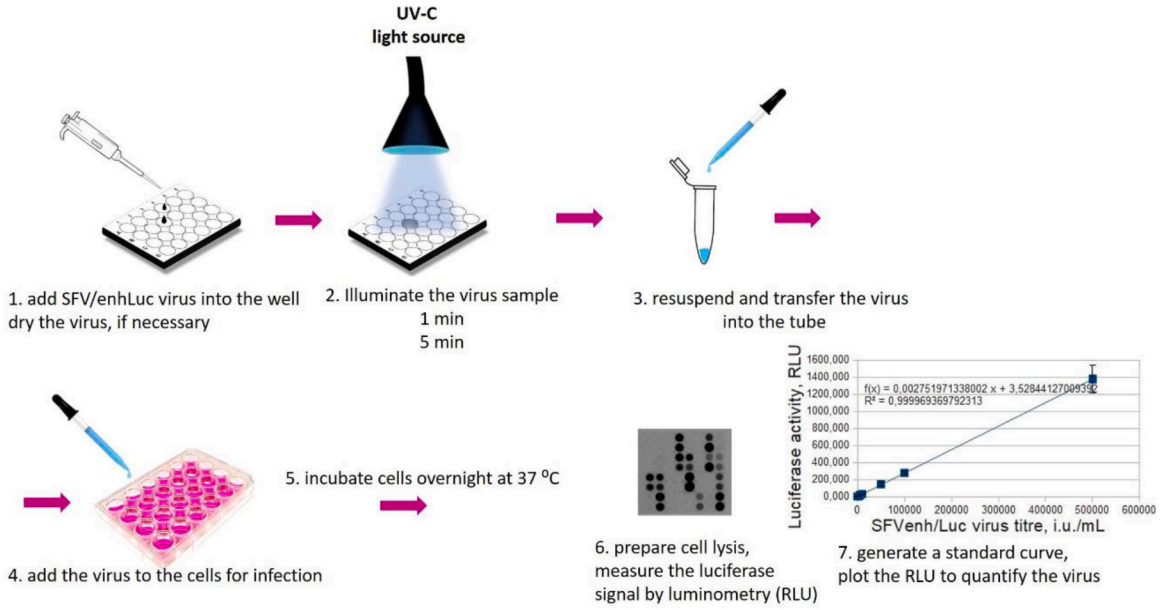

Fig. 8. Schematic illustration of the virus illumination test.

The prepared virus sample was fixed under the respective HFEL at a distance of 11 cm and irradiated for 1 or 5 min (Fig. 9). After the irradiation, the virus sample was mixed with PBS (containing Mg^{2+} and Ca^{2+}) to a final volume of 420 µl, added to the BHK-21 cells 200 µl per well in duplicate, and incubated with BHK-21 cells for 1 h at 37 °C, 5% CO_2, then 800 µl of BHK medium (1% fetal bovine serum) was added. In parallel, the standard dilutions of the SFVenh/Luc virus in a range of 5 × 10^5- 1 × 10^3 i.u. per well were generated and used for BHK-21 cell infection in duplicate in a 24-well plate. The cells were incubated overnight at 37 °C, 5% CO_2 to allow complete cell infection and firefly luciferase gene expression.

Changes in luciferase gene activity after virus UV irradiation were evaluated in comparison with the standard curve obtained from the virus standard dilutions. Relative light units (RLUs) were measured by the Luciferase assay (Promega), as recommended by the manufacturer. Briefly, the cell medium was removed and the cells (24-well) were lysed in 100 µl of the Cell Culture Lysis buffer (Promega), centrifuged at 3000 g for 5 min, and 2 µl of the cell lysate was used immediately for the measurement of the luciferase enzymatic activity by Luminometer (Luminoskan Ascent, Thermo Scientific, UK). The RLUs were calculated as an average mean of duplicates. The virus titre standard curve was generated in each experiment, and the negative control signal (RLU of uninfected cells) was subtracted from all values. The log10 reduction value (LRV) represents the difference between untreated (not illuminated) and illuminated virus titres i.u. per ml, and was calculated according to the following equation:

LRV = [log10 (virus titre without illumination) – log10 (virus titre after illumination)].

The example of the standard curve is presented in Supplementary material, Fig. S5.

2.4. Bacterial culture and growth conditions and disinfection experiments

For the inactivation tests, *E. coli* ATCC®1053 was prepared as reported previously [36]. For the inactivation tests, 3 ml of *E. coli* stock was inserted in a sterile 30 mm borosilicate Petri dish and placed under the lamp at a distance of 11 cm. For the forming of parallel light rays, a fused silica lens was used. The exposure time was changed from 1 to 10 min.

Immediately after irradiation, the sample was removed from the light source and decimal dilutions of the sample were inoculated onto Tryptone soya agar (Oxoid Ltd, UK) plates and incubated for 24 h at 37 °C. The result (reduction in cultivable *E. coli*) is expressed as negative log reduction of colony-forming units (CFU) after treatment divided by colony-forming units before treatment.

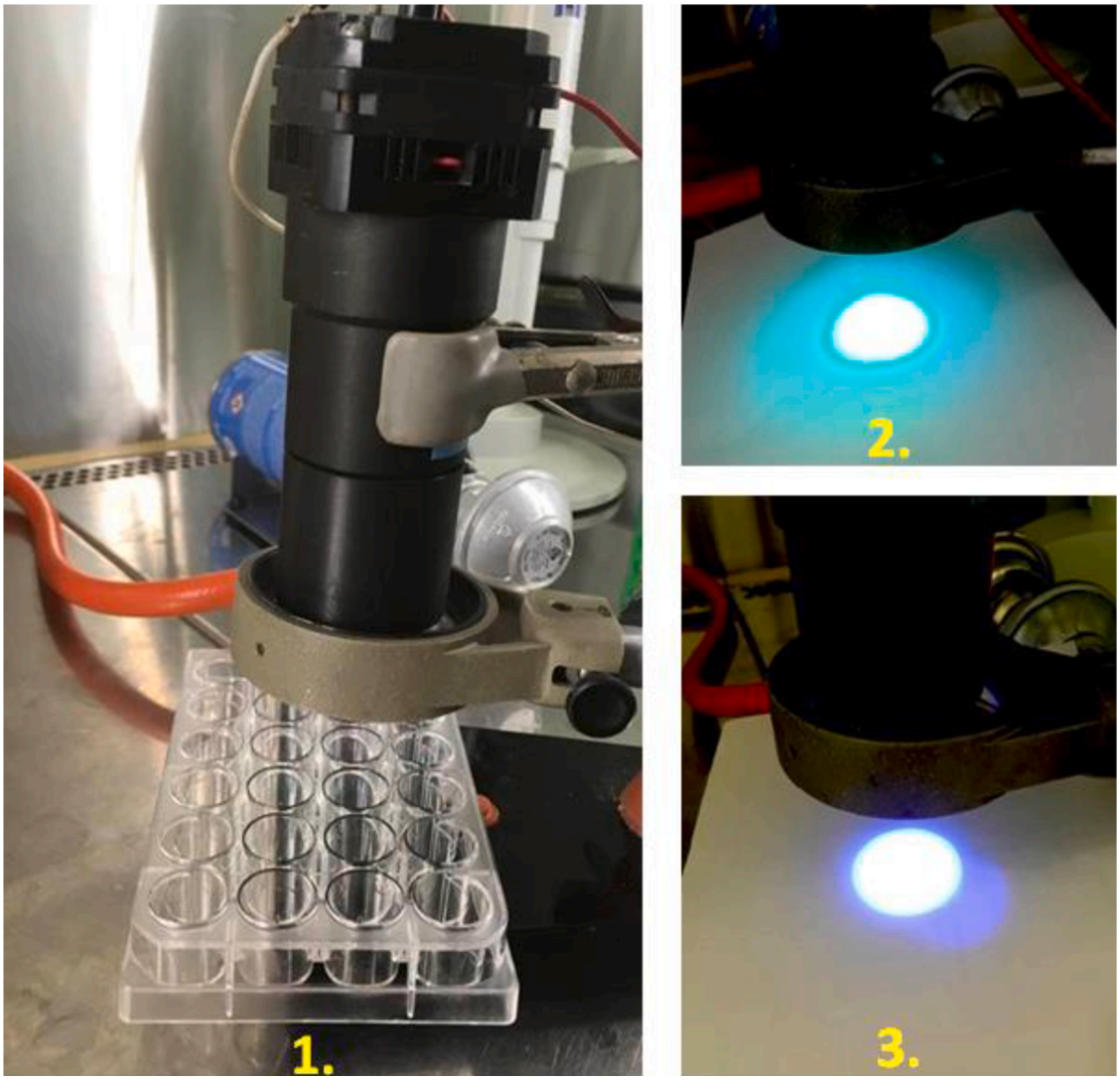

Fig. 9. 1) HFEL installation for virus illumination experiments, 2) Visible radiation from a thallium-antimony HFEL, 3) Visible radiation from a lead HFEL.

3. Results and discussion

The alternative polychromatic HFELs with thallium-antimony, arsenic, lead, selenium, and mercury fillings have been manufactured for the disinfection experiments. The irradiation tests were performed using calibrated Ocean Optics spectrometer HR4000+ as described in Methods. The obtained average integral intensity I_R (energy per unit surface area) of the light source over the illumination area (3 cm) in the UV-C was for mercury HFEL of 82.1 ± 4.8 μW/cm^2, thallium-antimony - 67.9 ± 7.0 μW/cm^2, arsenic - 79.5 ± 4.0 μW/cm^2, lead - 37.4 ± 11.7 μW/cm^2, selenium - 30.3 ± 11.0 μW/cm^2. The errors were calculated from at least 5 measurements.

UV dose D was calculated according to Eq (1) as intensity multiplied by time, and is expressed as mJ/cm^2. For example, the corresponding doses for Hg HFEL 1 min irradiation was 4.9 mJ/cm^2, 5 min - 24.6 mJ/cm^2, Tl-Sb 1 min - 4.1 mJ/cm^2, 5 min - 20.4 mJ/cm^2, Se 1 min - 1.8 mJ/cm^2, 5 min - 9.1 mJ/cm^2, Pb 1 min - 2.2 mJ/cm^2, 5 min - 11.2 mJ/cm^2.

3.1. Semliki Forest virus

To evaluate the UV irradiation disinfection efficiency, we have applied the recombinant SFV, which belongs to the enveloped single-stranded (+) RNA viruses (60 nm virus particle diameter) [37] structurally similar to other pathogenic viruses [38–40]. In this study, we used the test system based on a safe replication-deficient SFV1 vector (pSFVenh/Luc), allowing us to perform one round of cell infection without the synthesis of new progeny virions. The quantification of the virus was based on the measurement of luciferase activity in infected cells, which correlates with the virus dose, expressed in i.u. per ml. The SFV vector used in this study represents a genetically modified virus with natural envelope and replication-deficient genome, which does not contain virus structural genes [41]. The advantages of the recombinant SFV vector expressing the luciferase gene compared to the wild-type pathogenic human viruses include (i) biosafety allowing to work under BSL1/2 conditions and (ii) use of sensitive luciferase-based virus quantification in standard infection experiments.

Due to the absence of standard protocols of UV light germicidal activity evaluation for SFV, the efficiency of irradiation was evaluated in three different experimental settings, including two variants of viral suspension and with dried virus samples. Purified virus particle samples diluted in PBS buffer to 2 × 10^6 i.u. in 200 μl PBS (24-well plate), or alternatively 2 × 10^5 i.u. in 10 μl PBS (96-well plate), as well as dried virus particle sample 2 × 10^6 i.u. per sample (24-well plate), were used.

The virus sample was exposed to a HFEL, as described in methods, and the amount of the virus after irradiation was quantified and compared to the same control sample in a tissue plate not exposed to the UV light source. The virus quantification was performed by measurement of luciferase activity expressed as RLU in cell lysate after infection of BHK-21 cells with a corresponding virus sample. The virus titre was calculated by plotting respective RLUs onto the standard curve obtained by virus standard dilutions. The non-irradiated sample incubated at the same conditions was taken as 100%.

The results of the SFV/enhLuc virus inactivation are summarized in Table 2 and presented in Figs. 10–11.

The most efficient virus particle inactivation was observed in liquid samples in the 96-well plate after 5 min irradiation interval for thallium-antimony and mercury HFELs with almost complete virus inactivation (Table 2). For the Tl-Sb HFEL for the liquid 24-well plate after 5 min irradiation, the inactivation was even better than for Hg HFEL.

For the mercury lamp, the virus reduction log10 was in the range from 2.77 to >4.99, and for the thallium-antimony lamp, 3.10 to >4.99. In general, a higher reduction rate was calculated for the samples analysed in 96-well plate, because the overall volume and, accordingly, the amount of the virus particles was ten times lower, than in the 24-well plate (2 × 10^5 i.u. versus 2 × 10^6 i.u., respectively). According to the guidelines of the European Medicines Agency (CPMP/BWP/268/95,), the log10 reduction value is an important parameter to quantify the virus inactivation capacity, and only the log10 reduction >4 is advised as a "very high" reduction potential. Thus, in our experiment, similar to the standard mercury light source, the polychromatic thallium-antimony HFEL showed a very high reduction potential in the 96-well plate, and high reduction potential in the 24-well plate, which could be improved by enhancing the irradiation dose (exposure time) to the level, suggested being sufficiently high for practical disinfection requirements.

The observed differences in the inactivation kinetics of the mercury and thallium-antimony could be explained by different inactivation mechanisms and spectral behavior of the monochromatic 254 nm mercury HFEL and polychromatic thallium-antimony lamp. In Fig. 11 we can see that the LRV growth from the dose (slope) is faster for the

Table 2
The calculated virus reduction rates after exposure of SFV/enhLuc virus sample to different UV light sources. LRV - log10 reduction value.

Type of sample	Type of UV light source	Exposure time, min	Virus titre (i.u./ml± standard deviation)	Virus titre i.u. Log10	Virus titre reduction (Log10), LRV	Inhibition, %
Liquid, 24-well plate	Without irradiation)	–	(7.67 ± 0.62) x10^5	5.88	0	0.00
	Hg	5	(1.28 ± 0.27) × ·10^3	3.11	2.77	99.83
		1	(5.300 ± 0.699) × 10^4	4.72	1.16	93.09
	Pb	5	(1.09 ± 0.33) × 10^5	5.04	0.84	85.75
		1	(8.05 ± 3.34) × 10^5	5.91	0	0.00
	Tl-Sb	5	(6.04 ± 3.48) × 10^2	2.78	3.10	99.92
		1	(2.49 ± 0.07) × 10^5	5.40	0.48	67.52
	Se	5	(9.97 ± 0.22) × 10^4	5.00	0.88	87.00
		1	(2.96 ± 1.29) × 10^5	5.47	0.41	61.35
Liquid, 96 - well plate	Without irradiation	–	(9.68 ± 0.35) × 10^4	4.99	0	0.00
	Hg	5	0	>4.99	>4.99	100
	Pb	5	(2.2 ± 0.2) × 10^3	3.34	1.65	97.73
	Tl-Sb	5	0	>4.99	>4.99	100
Dry, 24-well plate	Without irradiation	–	(5.6 ± 2.3) × 10^3	3.75	0	0
	Hg	5	0	>3.75	>3.75	100
		1	(1.39 ± 0.25) × 10^3	3.14	0.61	75.14
	Pb	5	(3.76 ± 3.76) × 10^1	1.58	2.17	99.33
		1	(3.10 ± 0.33) × 10^3	3.49	0.26	44.60
	Tl-Sb	5	0	>3.75	>3.75	100
		1	(1.38 ± 0.23) × 10^3	3.14	0.61	75.34
	Se	5	(1.46 ± 0.12) × 10^3	3.16	0.59	74.01
		1	(4.01 ± 0.63) × 10^3	3.60	0.15	28.43

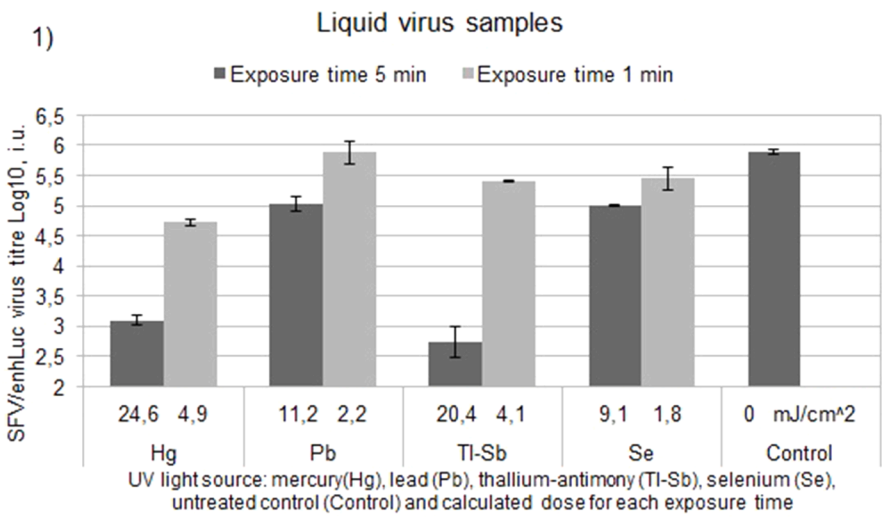

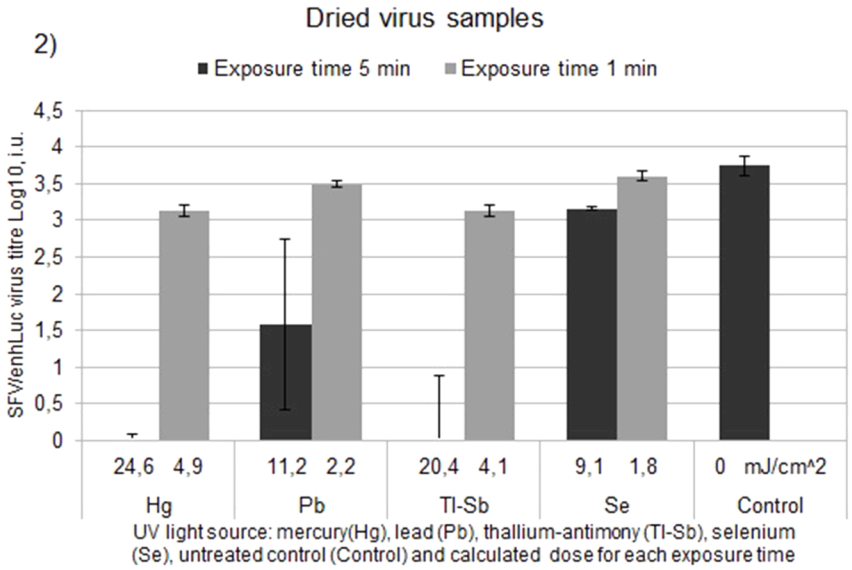

Fig. 10. Virucidal efficacy of UV irradiation. 1) A liquid layer of SFV/enhLuc virus-containing PBS solution (2×10^6i.u./200 µl in 24-well plate) was irradiated for either 5 min, or 1 min with respective HFEL and used for BHK-21 cell infection. 2) The SFV/enhLuc virus (1×10^6 i.u./20 µl in 24-well plate) was inoculated on the surface for 1 h to dry, then the dried spot was irradiated with respective HFEL (5 min and 1 min), afterword, soaked in a PBS buffer, resuspended and used for BHK-21 cell infection. The next day after infection, the cell lysates were prepared and luciferase light units were measured by luminometry. The virus titre was calculated according to the standard curve obtained by standard dilutions of SFV/enhLuc virus. Error bars represent the standard deviation of the mean of two independent experiments, each in duplicate. Untreated control - virus sample incubated in parallel (liquid, or dried) without irradiation.

thallium-antimony HFEL, especially in the liquid phase. That means that the rate constant *k* (Eq. (3)) is higher.

Using the lead HFEL having strong lines at about 217 nm and 220 nm and several weaker lines in the region from 245 nm - 280 nm, 2.17 log10 virus reduction was reached in 5 min exposure for dry samples (dose 11.2 mJ/cm^2). In contrast, the corresponding dose for mercury HFEL 5 min irradiation was about two times higher - 24.6 mJ/cm^2. For the Hg and Pb HFELs, if we qualitatively compare the rate constant (slope) from the LRV dependence on dose in Fig. 11, we see that in the case of the Pb HFEL the LRV grows faster from the applied dose than for the Hg HFEL (Supplementary material, Figs. S2–S3). It means that, in terms of rate constant *k*, Pb HFEL is also efficient. Increasing the exposure time, namely dose, the lead HFEL would also give a potentially high reduction value. The different decontamination rates can be explained by the different spectral compositions used, but this observation should be explored in more detail in the future. The selenium HFEL showed a considerably lower reduction potential. One of the explanations could be that the Se HFEL had lower intensity; however, the difference between intensities of the lead (37.4 ± 11.7 µW/cm^2) and selenium HFEL (30.3 ± 11.0 µW/cm^2) was not so substantial. Another explanation could be that here we observe the spectral influence on the inactivation process - lines below 220 nm have less effect on the inactivation than lines around 260 nm. Similar findings were observed by Beck et.al. [7] for bacteriophage MS2 and adenovirus.

To evaluate the efficacy of UV inactivation under different conditions resembling the natural environment, virus samples diluted in cell medium (DMEM) were dried and then irradiated. Interestingly, after drying the SFVenh/Luc virus samples lose their activity considerably. The composition of the virus-containing medium and drying conditions such as time and humidity can also influence the degree of the virus inactivation due to drying. There are data indicating that the high salt and protein content could have a protective effect on the viability of viruses [42], but on the other hand, the composition of the virus-containing medium could also influence UV light absorption. Furthermore, it was found that preparation of virus dilutions in cell medium such as DMEM versus PBS can affect the virus integrity during drying by unknown mechanism as it was discovered for enveloped bacteriophage phi6 [43]. For SFV samples, the initial amount of the virus was decreased for about 2.3 log10 (applied initially 1×10^6 i.u. per sample in the 24 well plate, after drying was detected as 5.6×10^3 i.u. only in comparison to standards). For the untreated control, the signal of 5.6×10^3 i.u. was detected at the level of the second lower standard point - 5×10^3, close to the detection limit, thus the comparison of samples under 10^3 score does not allow to distinguish minor differences of inactivation efficiency. Nevertheless, the data from irradiated dried samples showed the same general trend and sensitivity to UV light as the liquid virus

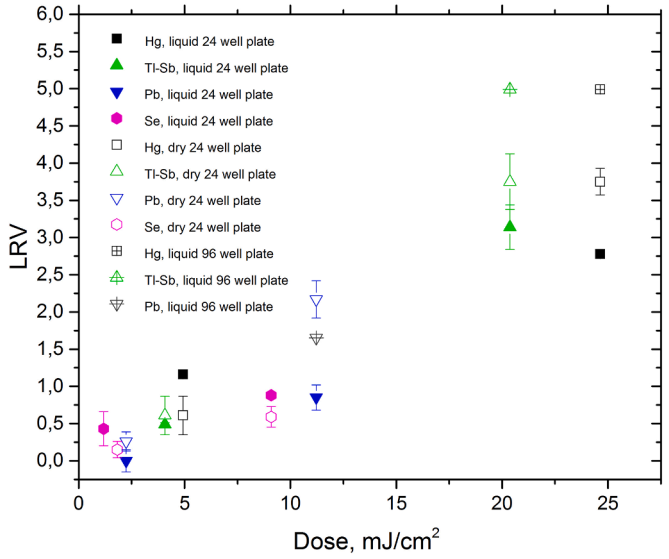

Fig. 11. SFV titre log10 reduction value LRV as a function of dose for different HFELs in different conditions, dry 24-well plate, liquid 24-well and 96-well plate.

samples.

The results presented in Fig. 10-11 and Table 2 show that the Tl-Sb HFEL with several peaks in the region from 200 - 277 nm offers an efficient inactivation of SFV, as the representative of enveloped RNA viruses. Also Pb HFEL showed a promising reduction rate that needs to be explored in the future in detail.

Comparing our results with the results of the Eischeid and Linden experiment [24] of the inactivation of adenoviruses type 2 with monochromatic and polychromatic UV-C light, we observed a similar trend - for polychromatic HFELs, the required dose was found to be lower than for monochromatic light.

In contrast to adenoviruses, which are more resistant to monochromatic low-pressure UV inactivation [24], the SFV particles were sensitive to both monochromatic and polychromatic HFELs. We can hypothesize that adenoviruses are stable due to a DNA genome, which can be repaired inside the cell after UV damage, moreover, the absence of lipid envelope, which potentially can be destroyed by UV irradiation by cross-linking and aggregation [44], make adenoviruses more resistant to irradiation, comparing to enveloped RNA viruses. Therefore, we could expect that UV doses cause significant structural changes in SFV envelope and RNA genome leading to the virus inactivation under treatment by monochromatic HFELs. This hypothesis is also supported by the study of RNA and DNA bacteriophages confirming that the single-stranded nucleic acid (ssRNA and ssDNA) viruses were more susceptible to UV inactivation than the viruses with double-stranded genome [45]. UV radiation is absorbed by RNA, which leads to the formation of pyrimidine dimers blocking the translation of plus strand RNA genome. The absence of the cell-dependent mechanism of RNA reparation leads to the crucial inhibition of virus replication, respectively [46].

The difference in UV effect (more precisely, in terms of the UV rate constant k) between dry and liquid samples have been observed also previously [1,12]. For example, it was observed that the UV rate constants were at least one order of magnitude smaller in aerosols than in liquids [1]. Some studies introduced species-dependent concept of UV rate constant k ratio aerosol and liquid to correlate the UV range of viruses in different phases. For example, UV rate constant k for coronavirus in the air is 1.8 - 6.0 times higher than that in liquid [47]. From the first estimation also in our case, the rate constant k is about 2.2 - 1.2 times higher in dry conditions than liquid, and it varies between applied light sources, for some light sources like Pb, Tl-Sb even giving higher values than for Hg after qualitative estimation. More data points are needed for more accurate calculations. It should be noted that PBS as a standard solvent (buffer) does not show any specific UV absorbance [48].

Thus, UV light can inactivate viruses in various environments with less adverse effects on target materials compared to chemical disinfectants. It has been shown previously that polychromatic UV can induce irreversible modification of nucleic acid, and denatures viral proteins and/or lipid bilayers of the viral envelope. Although the exact mechanism of virus inactivation by different wavelengths still remains to be determined, our study clearly demonstrates the virucidal effect of tested polychromatic UV light sources at a short exposure time.

3.2. Bacteria

Bacterial inactivation tests have been performed with Gramnegative bacterium - *E. coli* using thallium-antimony, arsenic, selenium, and mercury light sources. In Fig. 12, the reduction of bacteria depending on the exposure time is shown for three cases. The result (reduction in cultivable *E. coli*) is expressed as a negative log reduction of colony-forming units after treatment - C, divided by colony-forming units before treatment - C^0.

In addition to thallium-antimony, arsenic HFEL demonstrated high efficiency in the reduction of cultivable *E. coli*. We obtained 4 log10 reduction after 10 min of irradiation with the polychromatic thallium-antimony and arsenic HFELs. As a comparison, the mercury light source reached 4 log10 reduction in 3.4 min of exposure. In opposite, the selenium light sources did not demonstrate any disinfecting properties (< 90% reduction) and were excluded from further experiments.

In Fig. 13, 1, log reduction as a function of a dose is depicted. As it can be seen, the dependence of the growth of reduction from the dose shows quite similar behavior for all three light sources up to ~20 mJ/cm^2. For the mercury HFEL we can clearly observe so-called two-stage decay that can be described by the following equation [12, Page 54–56]:

$$N(t)_{total} = N(0)e^{-k_1 D} + N(t_1)e^{-k_2 D} \quad (5)$$

Where $N(t)_{total}$ is the total number of bacteria at the moment t, the first part shows the fast decay phase with the rate constant k_1 (that also for *E. coli* can be described by Eq. (2)), $N(t_1)$ is the number of bacteria subject to the slower decrease during tailing with the rate constant k_2.

It is commonly observed that there is a small fraction of the microbial

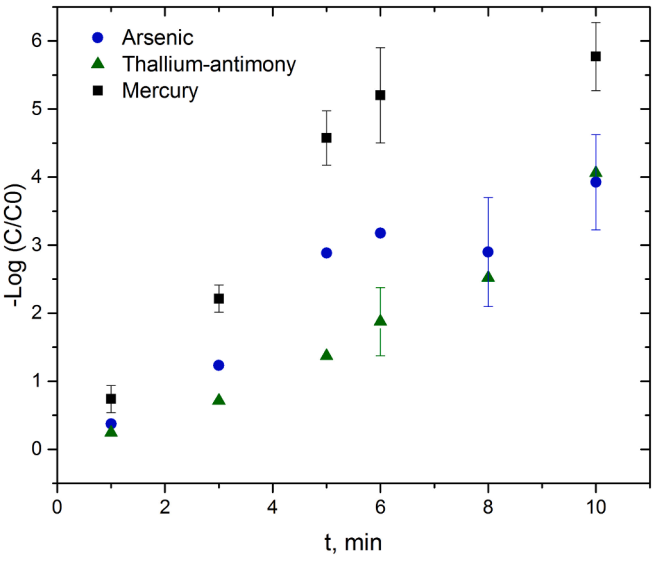

Fig. 12. Log10 reduction of *E. coli* CFU as a function of exposure time for HFELs by equal irradiation conditions.

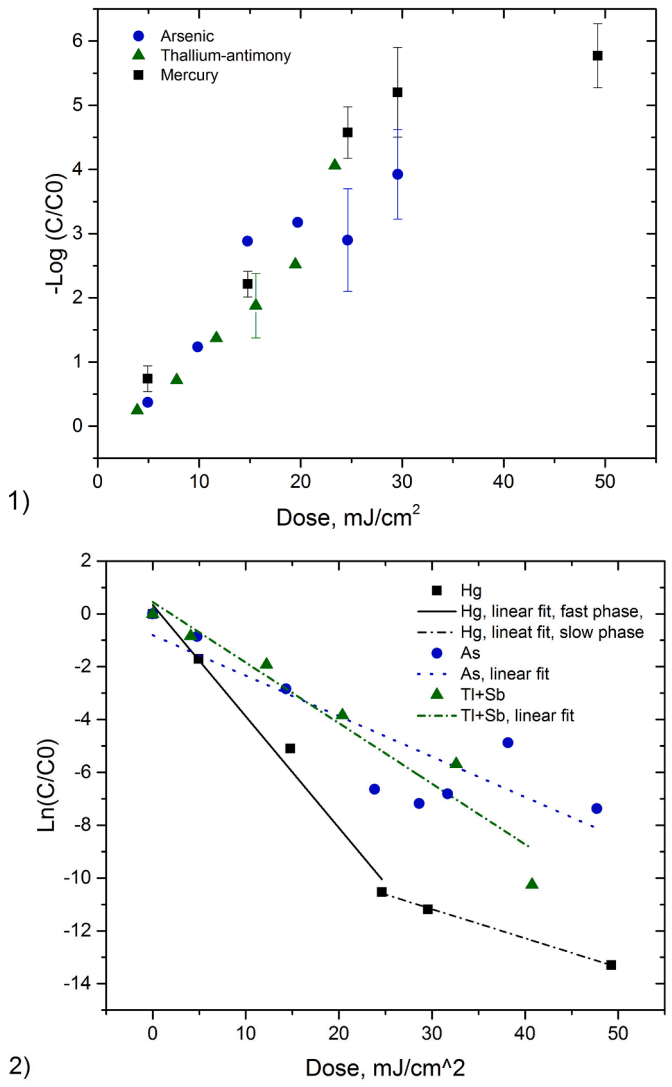

Fig. 13. 1) Log reduction of *E. coli* as a function from a dose, 2) Logarithm of survival S (Eq. (3)) as a function from irradiation dose for different light sources. The two-stage model for Hg HFEL - k_1=0.42 ± 0.04 cm^2/mJ (R^2=0.98), k_2=0.110 ± 0.004 cm^2/mJ (R^2=0.99); Tl-Sb HFEL - k = 0.23 ± 0.03 cm^2/mJ (R^2=0.94), As HFEL for one-stage linear fit - k = 0.17 ± 0.04 cm^2/mJ (R^2=0.84) but for two-stage plot k_1=0.27 ± 0.02 cm^2/mJ (R^2=0.98), k_2 =0.01 cm^2/mJ (R^2=1) (Supplementary material, Figs. S6-S10).

population that exhibits a higher level of resistance to UV radiation. There is a fast stage of decay in the beginning (first stage), where the most susceptible population is hit, and the second stage (slow decay) due to a more resistant population. This effect appears usually at 5 - 6 log10.

For the Tl-Sb and As HFELs the log reduction dependence from dose is linear (Fig. 13,2); however, for the As HFEL it seems that some tailing effect may begin at doses >30 mJ/cm^2. At least, fitting by taking into account the second stage gives better agreement with k = 0.17 ± 0.04 cm^2/mJ (R^2 = 0.84) for one-stage linear fit, but k_1 = 0.27 ± 0.02 cm^2/mJ (R^2 = 0.98), k_2 =0.01 cm^2/mJ (R^2 = 1) for the two-stage plot (Supplementary material, Figs. S8-S9). To decide whether it is true, more measurements at higher doses would be needed.

Not surprisingly, the results of Semliki Forest virus and *E.coli* inactivation tests were different due to differences in inactivation mechanisms. For example, Beck et.al. [7] observed different action results at the far UV-C wavelengths of bacteriophage MS2 (a common surrogate for enteric pathogens) and adenovirus. The authors showed that the damage of the nucleic acid at around 260 nm is the primary cause of inactivation for MS2. However, the spectral sensitivity of adenovirus diverged from the sensitivity of its genome below 240 nm, implying that nongenomic damage contributes to ultraviolet inactivation at these wavelengths.

As reported in [49], for *E. coli,* the main damaging mechanisms are bacterial DNA damage and oxidative stress. The currently used action spectrum for *E. coli* is not continued below 230 nm where typically protein absorption occurs. Also, we observed a strong influence of the spectral lines near the well-known maximum of the DNA absorption curve at 260 nm, causing mainly bacterial DNA damage (Hg 254 nm, Tl 277 nm, Tl 258 nm). However, arsenic HFEL is a different case also showing high-reduction effect, comparable to the mercury HFEL. The arsenic HFEL has only two weaker lines close to the DNA absorption band around 260 nm, namely, 275 nm and 278 nm. On the other hand, arsenic HFEL emits two strong lines at 230 nm, 235 nm, and spectral lines in the far UV-C region and beyond it with wavelengths 200 nm, 197 nm, 194 nm, possibly hitting the protein absorption band (Fig. 14) [50]. This interesting observed effect should be further investigated in the future.

Our experiments show that using polychromatic UV light sources offers a promising efficiency of inactivation of viruses and bacteria. This evidence could open a door to broader exploitation of polychromatic UV HFEL with non-mercury fillings. Furthermore, the high reduction potential of the HFELs shows that they potentially could be applied to other RNA viruses, including the SARS-COV-2 virus, as the reported doses of a mercury light source range from 3.7 mJ/cm^2 for 3 log reduction to 16.9 mJ/cm^2 for complete inactivation [2], which can be easily achieved.

4. Conclusions

In this work, new alternative polychromatic UV light sources, filled with arsenic, thallium-antimony, lead, selenium, emitting spectra in the UV spectral region from 190 nm - 280 nm, were produced and tested for inactivation of *E. coli* and Semliki Forest virus, a representative of human enveloped RNA viruses, as models of human pathogens. The thallium-antimony and arsenic-filled light sources showed a high pathogen inactivation effect.

For *E.coli*, 4 log10 reduction was obtained after 10 min of irradiation with both thallium-antimony and arsenic high-frequency electrodeless lamps. Main working lines of thallium-antimony HFEL at 258 and 277 nm are close to the DNA absorption curve peak at 260 nm, thus causing mainly bacterial DNA damage (similar to mercury 254 nm line). An even better result was obtained with arsenic HFEL having several intense lines at 230 nm, 235 nm, and in the far UV-C region and beyond it with wavelengths 200 nm, 197 nm, 194 nm, where the prime mechanism is supposed to be protein damage.

In the case of the Semliki Forest virus, the thallium-antimony UV light source demonstrated virus inactivation efficiency with a high virus reduction rate of 3.10 to > 4.99 log10 within 5 min of exposure. By our data, UV light from different sources is efficient in various environments, such as liquids and surfaces. We demonstrated that drying SFV samples strongly inhibits the infectivity of the virus, indicating the low environmental stability of the SFV. Nevertheless, the mercury and thallium-antimony irradiated dried virus samples showed a clear inactivation trend in comparison to selenium irradiated or non-irradiated dried virus samples. The high reduction potential of investigated HFELs shows that they potentially could be applied for inactivation of other structurally similar viruses, as reported doses of a mercury UV source for SARS-COV-2 virus inactivation range from 3.7 mJ/cm^2 to 16.9 mJ/cm^2 [2], which can be easily achieved.

The potential of lipid envelope damage by the polychromatic UV light sources should be considered for future research as efficient and less costly/energy-demanding mechanism of disinfection. The precise mechanism of action for different wavelengths of UV sources still have to be elucidated, despite the RNA damage presumably is the main, but not the only mechanism responsible for virus inactivation.

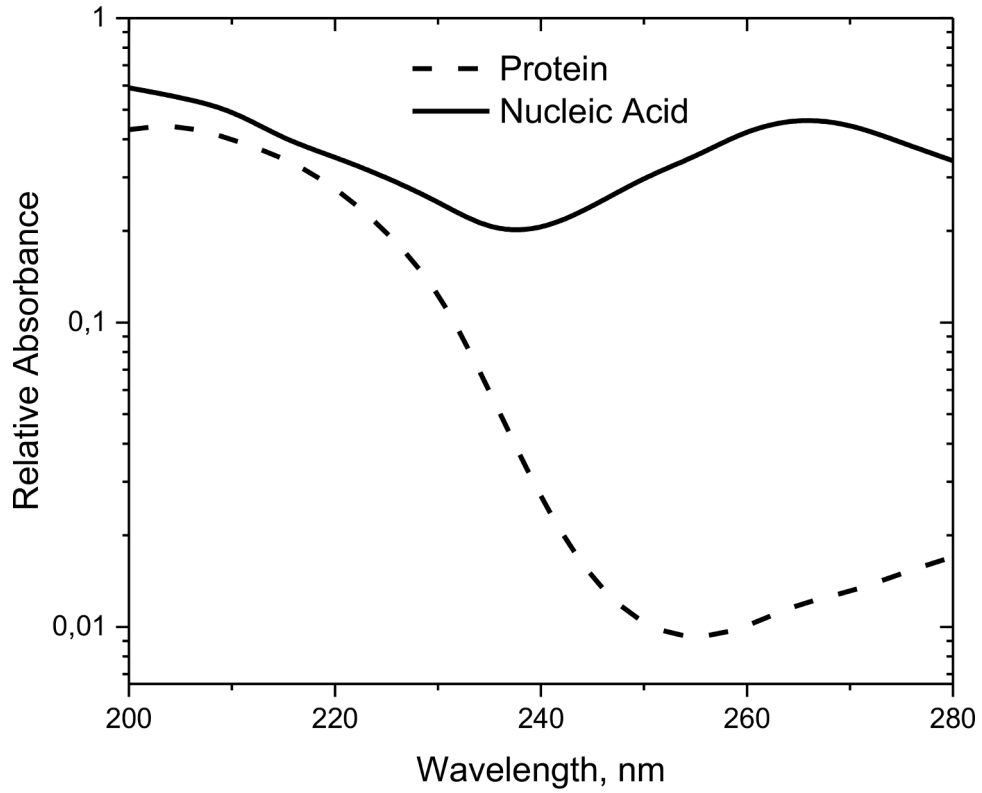

Fig. 14. Relative absorbance of proteins and nucleic acids from 200 nm to 280 nm [50].

Declaration of Competing Interest

The authors declare that they have no known competing financial interests or personal relationships that could have appeared to influence the work reported in this paper.

Acknowledgements

This research was partly financed from the project "Integration of reliable technologies for protection against Covid-19 in healthcare and high risk areas" VPP-COVID-2020/1–0004, the Latvian State research program. Authors acknowledge the Latvian Council of Science grant No. lzp-2020/1–0005 and the European Regional Development Fund (ERDF) grant No. 1.1.1.1/21/A/050. The authors thank Ms V.Denisova, Mr R.Vevers and K.Korotkaja for excellent technical assistance.

Supplementary materials

Supplementary material associated with this article can be found, in the online version, at doi:10.1016/j.jpap.2022.100120.

References

[1] H. Luo, L. Zhong, Ultraviolet germicidal irradiation (UVGI) for in-duct airborne bioaerosol disinfection: review and analysis of design factor, Build. Environ. 197 (2021), 107852.
[2] M. Biasin, A. Bianc, G. Pareschi, et al., UV-C irradiation is highly effective in inactivating SARS-CoV-2 replication, Sci. Rep. 11 (2021) 6260, https://doi.org/10.1038/s41598-021-85425-w.
[3] M. Heßling, K. Hönes, P. Vatter, C. Lingenfelder, Ultraviolet irradiation doses for coronavirus inactivation - review and analysis of coronavirus photoinactivation studies, GMS Hyg. Infect. Control 15 (2020) 1–8.
[4] Centres for Disease Control and Prevention, Implementing Filtering Facepiece Respirator (FFR) Reuse, Including Reuse after Decontamination, When There Are Known Shortages of N95 Respirators, Centers for Disease Control and Prevention (2020). https://www.cdc.gov/coronavirus/2019-ncov/hcp/ppe-strategy/decontamination-reuse-respirators.html. accessed 20 Oct 2020.
[5] T. Minamikawa, T. Koma, A. Suzuki, T. Mizuno, K. Nagamatsu, H. Arimochi, K. Tsuchiya, K. Matsuoka, T. Yasui, K. Yasutomo, M. Nomaguchi, Quantitative evaluation of SARS-CoV-2 inactivation using a deep ultraviolet light-emitting diode, Sci. Rep. 11 (2021) 5070.
[6] R.P. Rastogi, A. Richa, M.B.Tyagi Kumar, R.P. Sinha, Molecular mechanisms of ultraviolet radiation-induced DNA damage and repair, J. Nucleic Acids (2010), 592980.
[7] S.E. Beck, R.A. Rodriguez, M.A. Hawkins, T.M. Hargy, T.C. Larason, K.G. Linden, Comparison of UV-induced inactivation and RNA damage in MS2 phage across the germicidal UV spectrum, Appl. Environ. Microbiol. 82 (5) (2016) 1468–1474.
[8] A.C. Eischeid, K.G. Linden, Molecular indications of protein damage in adenoviruses after UV disinfection, Appl. Environ. Microbiol. 77 (3) (2011) 1145–1147.
[9] Y. Gerchman, V. Cohen-Yaniv, Y. Betzalel, S. Yagur-Kroll, S. Belkin, H. Mamane, The involvement of superoxide radicals in medium pressure UV derived inactivation, Water Res 161 (2019) 119–125.
[10] N.G. Reed, The history of ultraviolet germicidal irradiation for air disinfection, Public health rep 125 (1) (2010) 15–27.
[11] A. Su, S.M. Grist, A. Geldert, A. Gopal, A.E. Herr, Quantitative UV-C dose validation with photochromic indicators for informed N95 emergency decontamination, PLoS One 16 (1) (2021), e0243554.
[12] W. Kowalski, Ultraviolet Germicidal Irradiation Handbook, Springer Berlin Heidelberg, Berlin, Heidelberg, 2009.
[13] Absorbance Spectroscopy: Overview. In: G. Roberts, A. Watts, European Biophysical Societies (eds). Encyclopedia of Biophysics, Springer, Berlin, Heidelberg, 2018.
[14] H. Kitagawa, N. Toshihito, N. Tanuza, O. Keitaro, S. Norifumi, S. Takemasa, O. Hiroki, Effectiveness of 222-nm ultraviolet light on disinfecting SARS-CoV-2 surface contamination, Am. J. Infect. Control 49 (3) (2021) 299–301.
[15] M. Buonanno, D. Welch, I. Shuryak, D.J. Brenner, Far-UVC light (222 nm) efficiently and safely inactivates airborne human coronaviruses, Sci. Rep. 10 (2020) 10285.
[16] Y. Gerchman, H. Mamane, N. Friedman, M. Mandelboim, UV-LED disinfection of coronavirus: wavelength effect, J. Photochem. Photobiol. B 212 (2020), 112044.
[17] M. Raeiszadeh, F. Taghipour, Inactivation of microorganisms by newly emerged microplasma UV lamps, Chem. Eng. J. 413 (2021), 127490.
[18] T.P. Coohill, J.L. Sagripanti, Overview of the Inactivation by 254nm Ultraviolet Radiation of Bacteria with Particular Relevance to Biodefense, Photochem. Photobiol. 84 (2008) 1084–1090.
[19] A. Paradise, Reducing the Risk of Mercury Exposure For a Sustainable Future, My Green Lab®, San Diego, CA, USA, https://www.mygreenlab.org/uploads/2/1/9/4/21945752/mercury_light_source_education.pdf (assessed 16.01.2022).
[20] https://www.actionservicesgroup.com/blog/mercury-vapor-vs-led/. Assessed 16.01.2022.

[21] P. Maxson, M. Bender, A. Culver, Mercury in Fluorescent Lighting: unnecessary Health Risks & Actionable Solutions, Report Founded By Clean Lighting Coalition (CLiC) (2021) 1-40, Available https://cleanlightingcoalition.org/wp-content/uploads/sites/96/Mercury-in-Fluorescent-Lighting_FINAL-1.pdf (assessed 16.01.2022).
[22] https://www.mercuryconvention.org/en, assessed 16.01.2022.
[23] K.G. Linden, J. Thurston, R. Schaefer, P. James, Jr.J.P. Malley, Enhanced UV Inactivation of Adenoviruses under Polychromatic UV Lamps, Appl. Environ. Microbiol. 73 (23) (2007) 7571–7574.
[24] A.C. Eischeid, K.G. Linden, Protein damage in UV treated adenovirus. Water Quality Technology Conference and Exposition (2009) 3943–3949.
[25] G. Revalde, N. Zorina, A.Skudra J.Skudra, Diagnostics of capillary light sources by means of line shape measurements and modelling, J. Phys. Conf. Ser. 397 (1) (2012), 012070.
[26] G. Revalde, S. Sholupov, A. Ganeev, S. Pogarev, V. Ryzhov, A. Skudra, Use of radiaton sources with mercury isotopes for real-time highly sensitive and selectibve benzene determination in air and natural gas by direct differential absorbtion spectrometry with the direct Zeeman effect, Anal. Chim. Acta 887 (2015) 172–178.
[27] A.A. Ganeev, Z. Gavare, V.I. Khutorshikov, S.V. Khutorshikov, G. Revalde, A. Skudra, G.M. Smirnova, N.R. Stankov, High-frequency electrodeless discharge lamps for atomic absorption, Spectrochemica Acta B 58 (5) (2003) 879–889.
[28] G. Revalde, A. Skudra, Optimisation of mercury vapour pressure for the high-frequency electrodeless light sources, J. of Physics D: Applied Physics 31 (1998) 3343–3348.
[29] G. Revalde, A. Skudra, The HF-electrodeless light source cleaning method, In Proceedings HTMC-X, FSZ Jülich GmbH (2000) 301–304 .
[30] A. Ubelis, J. Silinsh, S. Putnina, A. Skudra, Manufacturing and investigation of the Electrodeless Discharge Lamps for UV and VUV Spectral Regions, 14th NASTEC, Naantali, Finland (1994) 58–59.
[31] S. Kazantsev, V.I. Khutorshchikov, G.H. Guthohrlein, L. Windholz, Creation of Highly Stable and Reliable Electrodeless Spectral Lamps, Practical Spectroscopy of High-Frequency Discharges, Plenum Press, New York and London, 1998, pp. 185–211.
[32] A. Svagere, J. Skudra, Intensity stability measurements of high-frequency electrodeless discharge lamps, 55th scientific conference for young students of physics and natural sciences: open readings 2012, 28-31 March 2012, Vilnius, Lithuania in Programme and abstracts, Vilnius University 49 (2012) 2029–4425. ISSN.
[33] B. Kurena, E. Müller, P.F. Christopoulos, I.B. Johnsen, B. Stankovic, I. Oynebraten, A. Corthay, A. Zajakina, Generation and functional in vitro analysis of Semliki Forest virus vectors encoding TNF-α and IFN-γ, Front. Immunol. 8 (2017) 1667.
[34] A. Zajakina, J. Vasilevska, D. Zhulenkovs, D. Skrastina, A. Spaks, A. Plotniece, T. Kozlovska, High efficiency of alphaviral gene transfer in combination with 5-fluorouracil in a mouse mammary tumor model, BMC Cancer 14 (1) (2014) 46.
[35] J. Vasilevska, D. Skrastina, K. Spunde, H. Garoff, T. Kozlovska, A. Zajakina, Semliki, Forest virus biodistribution in tumor-free and 4T1 mammary tumor-bearing mice: a comparison of transgene delivery by recombinant virus particles and naked RNA replicon, Cancer Gene Ther. 19 (8) (2012) 579–587.
[36] A. Skudra, L. Mezule, K. Spunde, G. Revalde, A. Zajakina, M. Zinge, T. Juhna, Alternative light sources for disinfection. ENVIRONMENT. TECHNOLOGIES. RESOURCES. Proceedings of the International Scientific and Practical Conference 1, Rezekne (2021) 2018–2222. http://journals.rta.lv/index.php/ETR/article/view/6596.
[37] J.H. Straus, E.G. Strauss, The alphaviruses: gene expression, replication, and evolution, Microbiol Rev 58 (3) (1994) 491–562.
[38] E. Hartenian, D. Nandakumar, A. Lari, M. Ly, J.M. Tucker, A.B. Glaunsinger, The molecular virology of coronaviruses, J. Biol. Chem. 295 (37) (2020) 12910–12934.
[39] Y.Z. Zhang, W.C. Wu, M. Shi, E.C. Holmes, The diversity, evolution and origins of vertebrate RNA viruses, Curr Opin Virol 31 (2018) 9–16.
[40] W.S. Ryu, Other Positive-Strand RNA Viruses, Molecular Virology of Human Pathogenic Viruses (2017) 177–184.
[41] P. Liljeström, H. Garoff, A new generation of animal cell expression vectors based on the Semliki Forest virus repli-con, Biotechnol J 9 (12) (1991) 1356–1361.
[42] K. Lin, C.R. Schulte, L.C. Marr, Survival of MS2 and Φ6 viruses in droplets as a function of relative humidity, pH, and salt, protein, and surfactant concentrations, PLoS One 15 (12) (2020), https://doi.org/10.1371/journal.pone.0243505.F.
[43] N. Rockey, P.J. Arts, L. Li, K.R. Harrison, K. Langenfeld, W.J. Fitzsimmons, A. S. Lauring, N.G. Love, K.S. Kaye, L. Raskin, B.Hegarty W.W.Roberts, K. R. Wigginton, Humidity and Deposition Solution Play a Critical Role in Virus Inactivation by Heat Treatment of N95 Respirators, mSphere 5 (5) (2020), https://doi.org/10.1128/mSphere.00588-20.
[44] R.M. Lawrence, J.D. Zook, B.G. Hogue, Full inactivation of alphaviruses in single particle and crystallized forms, J. Virol. Methods. 236 (2016) 237–244.
[45] C.C. Tseng, Ch. Sh, Li, Inactivation of viruses on surfaces by ultraviolet germicidal irradiation, J Occup Environ Hyg 4 (6) (2007) 400–405, https://doi.org/10.1080/15459620701329012.
[46] E.I. Budowsky, S.E. Bresler, E.A. Friedman, N.V. Zheleznova, Principles of selective inactivation of viral genome. I. UV-induced inactivation of influenza virus, Arch Virol 68 (3–4) (1981) 239–247.
[47] B. Beggs, E.J. Avital, Upper-room ultraviolet air disinfection might help to reduce COVID-19 transmission in buildings: a feasibility study, PeerJ (2020), https://doi.org/10.7717/peerj.10196.
[48] P. Yin, Y. Wang, Y. Qiu, L. Hou, Qin Liu, Y.R. Duan, Qiu Liu, Q. Li, Int. J. Nanomed. 7 (2012) 3961–3969, https://doi.org/10.2147/IJN.S3206.
[49] D. Pousty, R. Hofmann, Y. Gerchman, H. Mamane, Wavelength-dependent time-dose reciprocity and stress mechanism for UV-LED disinfection of Escherichia coli, J. Photochem. Photobiol. B 217 (2021), https://doi.org/10.1016/j.jphotobiol.2021.112129, 112129,ISSN1011-1344.
[50] W. Harm, Biological Effects of Ultraviolet Radiation, University Press, United Kingdom, 1980. http://inis.iaea.org/search/search.aspx?orig_q=RN, 12595451.